Low temperature processed NiOx hole transport layers for efficient polymer solar cells

Sudam D. Chavhan, Rickard Hansson, Leif K. E. Ericsson, Paul Beyer, Alexander Hofmann, Wolfgang Brütting, Andreas Opitz, Ellen Moons

Angaben zur Veröffentlichung / Publication details:

Chavhan, Sudam D., Rickard Hansson, Leif K. E. Ericsson, Paul Beyer, Alexander Hofmann, Wolfgang Brütting, Andreas Opitz, and Ellen Moons. 2017. "Low temperature processed NiOx hole transport layers for efficient polymer solar cells." *Organic Electronics* 44: 59–66. https://doi.org/10.1016/j.orgel.2017.01.040.

Organic Electronics, 44 (2017) 59-66 https://doi.org/10.1016/j.orgel.2017.01.040

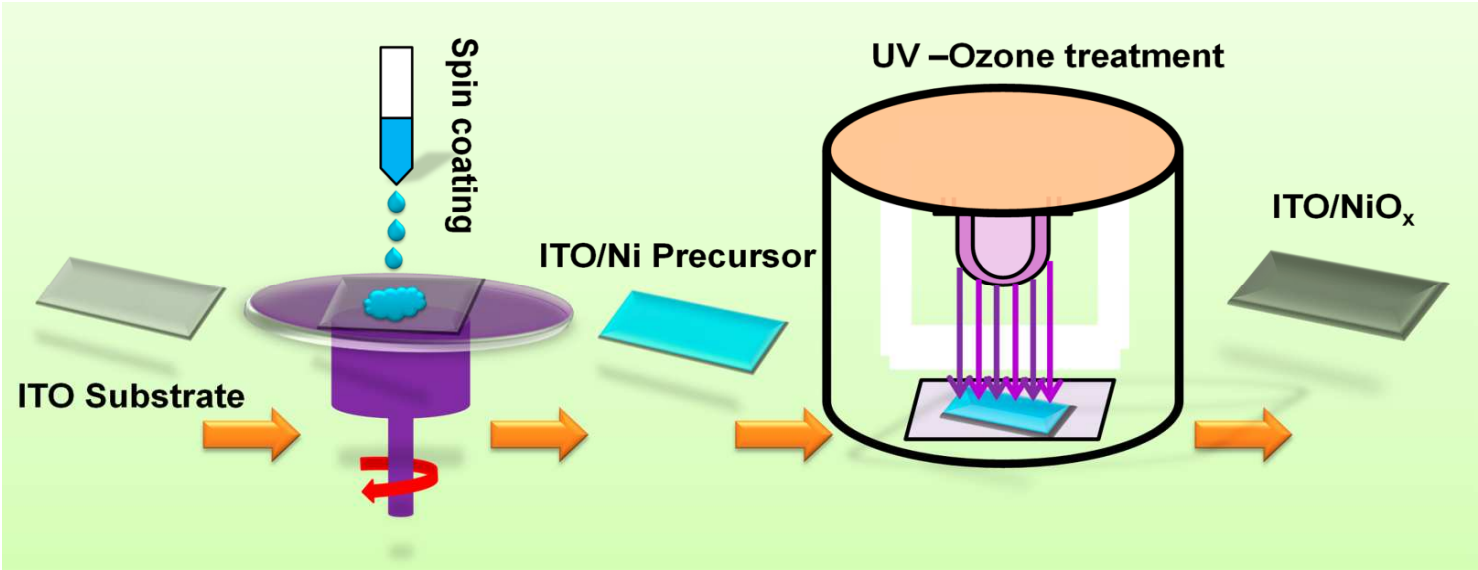

Organic Electronics, 44 (2017) 59-66 https://doi.org/10.1016/j.orgel.2017.01.040

Low temperature processed NiO_x hole transport layers for efficient polymer solar cells

Sudam D. Chavhan,[a*†] *Rickard Hansson,*[a†] *Leif K. E. Ericsson,*[a] *Paul Beyer,*[b] *Alexander Hofmann,*[c] *Wolfgang Brütting,*[c] *Andreas Opitz,*[b] *Ellen Moons*[a‡]

[a]Department of Engineering and Physics, Karlstad University, 65188 Karlstad, Sweden
[b]Department of Physics, Humboldt-Universität zu Berlin, 12489 Berlin, Germany
[c]Institute of Physics, University of Augsburg, 86135 Augsburg, Germany
[*]Present address: Department of Chemical Engineering, National Taiwan University, 10617 Taipei, Taiwan.
[†]SDC and RH have contributed equally to the work.
‡Corresponding author. e-mail address: ellen.moons@kau.se

Keywords: OPV; Nickel oxide; Hole injection layer; UV-ozone; Kelvin probe; XPS

Abstract

We here demonstrate the use of solution processed NiO_x thin films as the hole transport layer (HTL) in a thiophene–quinoxaline copolymer:fullerene solar cell. The NiO_x films, which are prepared by UV-ozone treating a nickel formate precursor, outperform the solar cells prepared in this study that use PEDOT:PSS as HTL. The power conversion efficiency improves from 5.3% to 6.1% when replacing PEDOT:PSS with NiO_x. Unlike most conventional ways of fabricating solution processed NiO_x HTLs, our method does not require high temperature (>300°C). In fact, we were able to produce high performing NiO_x HTLs without the use of any thermal annealing. X-ray photoelectron spectroscopy revealed that a mixture of oxides and hydroxides is formed as a result of the UV-ozone treatment, which differs in composition from those formed by high temperature annealing; UV-ozone treatment produces NiOOH, while only the high temperature annealing produces any significant amount of NiO. Contact

potential difference (CPD) measurements reveal an increased work function for all UV-ozone treated NiO_x films, consistent with the presence of NiOOH at the surface. The high work function of the UV-ozone treated NiO_x films leads to an improved energy level matching between the donor and the HTL, resulting in higher fill factor and hole injection current.

1. Introduction

Polymer solar cells are promising as a technology to produce clean energy from the abundant and freely available solar energy because of their low production cost owing to the compatibility with low temperature deposition processes by roll-to-roll printing for large scale production, the possibility to make flexible, light weight devices and record power conversion efficiencies (PCE) exceeding 10% for single-junction devices.[1-6] To commercialize this technology, it is of paramount importance to further increase the PCE and to insure long term stability, i.e. minimum 5-7 years operation lifetime of the solar cells.[7] One of the ways to improve both the performance and stability of polymer solar cells is to use metal oxides as hole transport layers (HTL) instead of the commonly used poly(3,4-ethylenedioxythiophene) polystyrene sulfonate (PEDOT:PSS).[8, 9] Even though PEDOT:PSS meets all the technical requirements for rapid low cost production of polymer solar cells, its inherent acidic and hygroscopic properties have been proven to be a major cause of degradation in organic photovoltaics (OPV).[10-14]

High work function metal oxides are suitable candidates as HTL materials; MoO_3,[15-19] V_2O_5,[20, 21] CuO_x,[22] WO_3,[23, 24] and IrO_x[25] have all been reportedly used in OPVs. Another metal oxide showing great promise as HTL material is NiO_x. NiO_x has been deposited by several different methods, such as pulsed-laser deposition,[26, 27] thermal evaporation,[28] atomic layer deposition,[29, 30] sputtering[31, 32] and solution processing.[33-37] Avoiding deposition techniques that require vacuum is desirable for low cost OPV fabrication and therefore solution-processed NiO_x is an advantageous. However, so far, high performance solar cells using solution processed NiO_x HTL, require often high annealing temperature.[33, 35-37] Stable and efficient polymer solar cells using solution processed NiO_x HTLs have previously been demonstrated by Steirer et al., who thermally annealed a NiO_x precursor at 300°C followed by exposure to O_2-plasma treatment.[33] The study revealed that the O_2-plasma treatment increased

the work function of the NiO_x, leading to improved device performance compared to solar cells with PEDOT:PSS as HTL. Recently Zhai et al. reported on UV-ozone treatment as a method to produce NiO_x HTLs at low temperature (<150°C).[38] Simultaneous thermal annealing and UV-ozone treatment of a nickel acetate precursor resulted in solar cells that outperformed devices using PEDOT:PSS HTL, mainly due to an increased fill factor (FF). Another way to produce NiO_x thin films at low temperature or room temperature is to use NiO_x nanoparticles, as was recently shown by Jiang et al. who achieved improved or comparable performance in polymer solar cells compared to PEDOT:PSS.[39]

UV-ozone treatment of oxide surfaces is known to lead to higher work functions.[38, 40-42] Here we report on the development of a method to grow NiO_x films from a nickel formate precursor solution at low temperature (even as low as room temperature) by a post deposition UV-ozone treatment. Using NiO_x as HTL, improved performance was demonstrated for bulk heterojunction polymer solar cells using poly[2,3-bis-(3-octyloxyphenyl)quinoxaline-5,8-diyl-alt-thiophene-2,5-diyl] (TQ1),[43] mixed with the fullerene derivative [6,6]-phenyl C_{71}-butyric acid methyl ester ($PC_{70}BM$).

2. Experimental Section

2.1 Materials

PEDOT:PSS (Clevios P VP AI 4083) was purchased from Heraeus Precious Metals GmbH & Co. KG and filtered through a 0.45 µm nylon filter prior to spin coating. The synthesis of TQ1 is described elsewhere.[43] The number average and weight average molecular weights were M_n = 34 kg/mol and M_w = 91 kg/mol, determined by size exclusion chromatography relative to polystyrene standards. $PC_{70}BM$ (purity > 99%) was purchased from Solenne BV (The Netherlands). Nickel formate dihydrate (99.9%), anhydrous ethylene glycol (99.8%) and ethylenediamine (>99.5%) were purchased from Alfa Aesar, Sigma-Aldrich and Fluka

analytical, respectively. Ortho-dichlorobenzene (oDCB) of analytical grade and 1-chloronaphthalene (CN) of technical grade were purchased from Sigma-Aldrich and used as received.

2.2 Preparation of the hole transport layer

Patterned ITO-coated glass substrates (Kintec Company, China) with a 200 nm thick ITO layer and sheet resistivity of 10 Ω sq^{-1} were cleaned in isopropanol in an ultrasonic bath and UV-ozone treated for 20 min. For the samples with PEDOT:PSS as the HTL, 50 nm of PEDOT:PSS was deposited by spin coating followed by thermal annealing at 120°C in a low vacuum oven for 20 min to remove any remaining water. For the NiO_x HTL deposition, a 37 mg/ml solution of nickel formate dihydrate was prepared in ethylene glycol and ethylene diamine was added such that a 1:2 (mol/mol) nickel formate dihydrate: ethylene diamine molar ratio was obtained. The solution was stirred on a hot plate at 100°C overnight and then spin coated onto the cleaned ITO substrates at 7000 rpm for 90 s. The ITO/NiO_x samples were then either given different heat treatments ranging from 100-325°C in ambient air or were kept at room temperature. Some of the ITO/NiOx were subsequently exposed to UV-ozone for 3 h using a PSD-UV cleaner (Novascan technologies, USA). Atomic force microscopy (AFM) images of ITO and ITO/NiO_x films can be found in Figure S1 of the supplementary material. The difference in surface morphology between the bare ITO and the ITO/NiO_x is not significant, indicating that the NiO_x layer is thin and homogenous. The NiO_x thickness was estimated by AFM by making a scratch in the NiO_x film and measuring the step height, and by scanning electron microscopy by cleaving the NiO_x-covered substrate and imaging the cross section. This way, we find the thickness to be in the range of 5-10 nm.

2.3 Device fabrication and J-V-characterization

The solar cell structure is glass/ITO/HTL/TQ1:$PC_{70}BM$/LiF/Al. Blend solutions of TQ1:$PC_{70}BM$ in a 1:3 weight/weight ratio, at a total concentration of 29 mg/ml, were prepared in oDCB, with the addition of 5 % (vol) of CN. The active layer was deposited on the ITO/HTL substrates by spin coating at 500 rpm for 100 s in a protected N_2 atmosphere (<0.1 ppm O_2, <0.1 ppm H_2O) inside a glove box (M. Braun Inertgas-Systeme GmbH). The active layer thickness, 100 ± 5 nm, was measured by scanning across a scratch in the film with the tip of an AFM (Nanoscope IIIa Multimode, Veeco Metrology group, now Bruker Corporation). After spin-coating the active layer, the samples were transferred to the vacuum chamber of the thermal evaporator (Univex 350 G, Oerlikon Leybold Vacuum GmbH) integrated in the glove box, where nominally 0.3 nm LiF and 100 nm Al were deposited with a deposition rate of 0.5 Å s^{-1} (LiF) and 1 Å s^{-1} (Al) at 10^{-6} mbar. The active area of the devices was 8 mm^2. The ITO is patterned and the HTL material covers the entire area, except for the areas where external contact is made to the ITO. The pixels on each substrate share the same ITO electrode, but have individual Al electrodes. The current-voltage characteristics of the solar cells were measured using a Keithley 2636A SourceMeter under illumination from an AM 1.5 solar simulator (Sol2A, model 94022A, Oriel Instruments, USA), with an intensity of 100 mW cm^{-2}, determined by a standard silicon photodiode. The solar cells were protected from air by mounting them in a sealed cell before taking them out of the glove box. As a consequence the solar cells were illuminated through the 2 mm thick poly(methyl methacrylate) (PMMA) cover window of the cell. No spectral correction was made for any UV light absorption by the PMMA. No apertures were used for the JV measurements. However, the EQE integrated over the solar spectrum agrees with the Jsc. When extracting the photovoltaic parameters, the data points were interpolated using a cubic spline.

EQE measurements were performed using a halogen light source (Müller Elektronik-Optik) in conjunction with a monochromator (Zolix Omni-λ 300). The light beam is split with a Y-fiber

and the reference arm fitted to a silicon photodiode of known EQE is measured with a Keithley 237 source meter. The other beam is chopped and hits the device, which is placed in an evacuated cryostat. To avoid detection of residual stray light the photocurrent is measured by a lock-in amplifier (Stanford SR830).

2.4 Materials characterization

The composition of the NiO_x layers was studied by X-ray photoelectron spectroscopy (XPS), performed at beamline D1011 of the MAX-IV National Laboratory for Synchrotron Radiation in Lund, Sweden. The photoelectrons were collected in normal emission using a SCIENTA SES200 electron-energy analyzer. All spectra were energy calibrated with respect to the Fermi level measured on a gold surface that had been cleaned in situ by argon sputtering. Survey scans and Ni 2p spectra were acquired using a photon energy of 1000 eV, O 1s spectra using 590 eV. All spectra were normalized to photon flux and a Shirley background was removed from the core-level spectra. Voigt profiles were used for the fitting.

UV-Vis absorption and reflection spectroscopy were performed using a Cary 5000 UV-Vis-NIR spectrophotometer (Agilent Technologies, USA), equipped with an integrating sphere.

Work function measurements were done with an ambient Kelvin probe (SKP5050 from KP technology Ltd.), using a vibrating gold reference electrode. The contact potential difference for a gold reference sample was determined to be +30 mV. The work function of this reference sample was measured by a photo-yield spectrometer AC-2 by Riken Keiki) as 4.8 eV. Additional activation of the surface was realized by home-build UV lamp.

3. Results and discussion

Solar cells were prepared with TQ1:$PC_{70}BM$ (1:2) spincoated from oDCB + 5% CN as the active layer, using NiO_x HTL and compared to reference samples with a PEDOT:PSS HTL.

The photovoltaic parameters for these devices, with NiO HTL layers annealed at different temperatures, with and without UV-ozone treatment, are shown in Table 1 and current-voltage (JV) curves, measured under AM 1.5 illumination, are shown in Figure 1a-c. The devices with NiO_x HTL without UV-ozone treatment exhibit poor photovoltaic performance and the open circuit voltage (Voc) varies strongly with the annealing time. Not until the annealing temperature is increased to 325°C can we observe any significant improvements of the solar cell performance. In Figure 1a, JV-curves are shown for solar cells with a NiO_x HTL annealed at 175°C for 24 h, 325°C for 30 min, and 325°C for 2 h, respectively, without UV-ozone treatment. Since annealing at 325°C also increases the sheet resistivity of the ITO (a 40% increase was measured after annealing at 325°C for 4 h), prolonging the annealing time further is not desirable.

As seen in Table 1 and Figure 1b, 3 h of UV-ozone treatment dramatically increases the device performance, mainly due to an increased fill factor (FF). All UV-ozone treated NiO_x samples, those annealed at all of the used temperatures, as well as those kept at room temperature, show a high performance. The corresponding JV-curves are shown in Figure 1b. For the devices with UV-ozone treated NiO_x, the Voc is larger (0.85-0.88 V) and not significantly affected by the annealing time, in contrast to the NiO_x-based devices without UV-ozone treatment.

Among all the UV-ozone treated NiO_x samples, those annealed at 175°C gave the highest performance. The best performing cell displayed a short circuit current density (J_{SC}) of 10.3 mA/cm^2, V_{OC} 0.87 V, FF 71.3% and PCE: 6.39%, which is compared in Figure 1c to a similar solar cell where NiO_x is replaced by PEDOT:PSS. All the UV-ozone treated NiO_x layers give a higher FF than the PEDOT:PSS-based reference devices we prepared in this study. The FF can be influenced by parasitic resistances as well as the charge injection. The series resistances of the devices were obtained by fitting the modified Shockley equation[44] to the

high voltage part of the dark JV-curves and was found to be ~4 $\Omega \cdot cm^2$ for the devices with PEDOT:PSS, all the UV-ozone treated NiO_x as well as the 325°C annealed NiO_x without UV-ozone. Hence the series resistance is not the reason for the difference in FF for NiO_x and PEDOT:PSS, and indicates that these HTL films have similar conductivities. The parallel resistance, obtained from the inverse slope of the dark JV-curves close to zero voltage, on the other hand is higher for the NiO_x devices (average $6 \cdot 10^6$ $\Omega \cdot cm^2$) than for PEDOT:PSS (average $4 \cdot 10^5$ $\Omega \cdot cm^2$). However, this has a negligible effect on the shape of the light JV-curves. Therefore, the differences between the FF for NiO_x and PEDOT:PSS can be assigned to differences in charge injection. Indeed, the dark JV-curves (Figure 1c) show that the forward current is higher for the NiO_x than for the PEDOT:PSS-based devices, indicating more efficient charge injection. The external quantum efficiency (EQE) spectra of the devices, measured at short-circuit conditions, are shown in Figure 1d. The J_{SC} calculated by integrating the EQE together with the AM 1.5 solar spectrum gave 9.76 mA/cm^2 for NiO_x and 9.96 mA/cm^2 for PEDOT:PSS, a difference within less than 6% of the J_{SC} mean values obtained from the JV-measurements.

Since the light is incident on the solar cell through the ITO/HTL contact, the HTL layers should have a high transmittance. Optical properties of the NiO_x layers are depicted in Figure 2. Figure 2a shows the optical transmittance in the wavelength range 200-800 nm of NiO_x layers annealed at different temperatures (100°C and 175°C for 24 h, 325°C for 30 min) with and without subsequent UV-ozone treatment. These spectra are measured on films on quartz substrates, and the transmittance of the layers are shown in Figure 2a. Prior to UV-ozone treatment, the transmittance is close to 100% in the visible range, while the UV-ozone treatment reduces the transmittance to just above 90%.

In Figure 2b the transmittance and reflectance spectra of a blank ITO/glass substrate are compared to ITO covered by PEDOT:PSS, and to ITO covered by untreated and UV-ozone treated NiO_x annealed at 175°C. The spectra of the blank ITO sample and the ITO/NiO_x sample without UV-ozone treatment look very similar. The NiO_x sample that was UV-ozone treated transmits slightly less light. The PEDOT:PSS covered ITO/glass in fact transmits more light than the blank ITO/glass substrate for wavelengths in the range from 375 nm to 550 nm. The explanation for this can be found in the reflectance measurement, shown in the same figure, where it can be seen that the PEDOT:PSS covered ITO/glass reflects less light than just ITO/glass in that range.

Comparing the optical properties of the UV-ozone treated NiO_x to PEDOT:PSS, the slightly higher J_{SC} observed in solar cells using PEDOT:PSS (Table 1 and Figure 1) can be rationalized by the higher optical transparency shown in Figure 2b.

XPS measurements were performed to analyze the chemical composition at the surface of the NiO_x films. XPS survey scan spectra of the NiO_x films deposited on Si/SiO_x substrates are shown in Figure 3. Spectra of UV-ozone treated NiO_x films are shown for different annealing temperatures prior to the UV-ozone treatment and are also compared to NiO_x films annealed to 325°C without any subsequent UV-ozone treatment. Characteristic peaks from nickel, oxygen, and carbon are clearly visible. The unannealed UV-ozone treated NiO_x film contains less carbon than the films that have been annealed and has also a visible Si 2p peak from the underlying substrate, showing that the UV-ozone treatment removes more material when applied on the unannealed NiO_x film than on the pre-annealed films. In the spectra of the other UV-treated NiO_x films shown in Figure 3, the nickel and oxygen peaks get more pronounced as the annealing temperature increases and no traces of silicon are visible, thus showing that the NiO_x film is fully covering the substrate. Also the C1s peak grows somewhat as the annealing temperature increases. When comparing the 325°C sample with and without

UV/ozone treatment, we can clearly see that the UV-ozone treatment removes part of the carbon, even on the annealed samples, but it doesn't remove it completely, indicating that the carbon get bound to the film upon annealing.

Figure 4 shows the Ni $2p_{3/2}$ and O 1s XPS spectra of the NiO_x thin films. In the Ni $2p_{3/2}$ spectra, the broad peak centered at approximately 7 eV higher binding energy than the main peak has been assigned to final state effects.[45, 46] Figure 4a and b show the spectra of a film of the NiO_x precursor. In order to remove any residual ethylene glycol (boiling point 197°C), the film had been heated to 175°C, which is below the decomposition temperature of the nickel formate precursor.[47, 48] The O 1s spectrum (4b) shows a single symmetric peak that was fitted to a single component, indicating that the oxygen present in the film is likely to originate from the nickel formate that indeed has not been decomposed. Thus we assign this peak to nickel formate.

The NiO_x film heated to 325°C without subsequent UV-ozone treatment displays a distinct NiO peak at 853.4 eV in the Ni $2p_{3/2}$ spectrum and 529.6 eV in the O 1s spectrum; the peak positions being in agreement with previous reports.[30, 36, 38] The peak at 855.1 eV in the Ni $2p_{3/2}$ spectrum and 531.5 eV in the O 1s spectrum could be due to either $Ni(OH)_2$ or Ni_2O_3, the peak has previously been assigned to both species.[36] In the O1s spectrum, on the higher binding energy side of the $Ni(OH)_2/Ni_2O_3$ peak, at least one more species is clearly present. In the $Ni2p_{3/2}$ spectrum this is not as clearly visible due to partial overlap from the broad peak assigned to final state effects. Following the procedure of Zhai et al,[38] a single component could be fitted at 856.6 eV (Ni $2p_{3/2}$) and 533.3 eV (O 1s) which we assign mainly to NiOOH. This position is at ~1 eV higher binding energy than what is reported in the literature for NiOOH, although we note that those reported values themselves differ by about 1 eV.[34, 36, 38] For this reason we cannot completely exclude the possibility that the component which we assign to NiOOH also could have some contributions from any undecomposed precursor

(Figure 4b) or physisorbed water which both would appear at slightly higher binding energy than NiOOH (see Figure 4b and ref. 34). However, the reduced optical transmission and visible colour change of the NiO_x films upon UV-ozone treatment, shown in Figure 2a, corroborates our interpretation that NiOOH is formed during the UV-ozone exposure, since NiOOH is known to be a black solid.

For the NiOx films heated to 325°C, both the O 1s and Ni $2p_{3/2}$ spectra are shifted towards lower binding energies compared to the lower temperature NiO_x films, which we interpret as a shift of the Fermi level. This interpretation is strengthened by the observation of a similar shift of the valence band towards the Fermi level, shown in Figure S2 of the supplementary material.

For the UV-ozone treated NiOx films, the chemical composition varies depending on the preceding thermal annealing. The Ni $2p_{3/2}$ and O 1s spectra of UV-ozone treated, unannealed NiO_x films (Figure 4c and 4d) are quite broad, showing that several different nickel and oxygen containing species are present. Since the XPS survey scan of this film (Figure 3) showed peaks from the Si/SiO_x substrate, this O 1s spectrum also contains SiO_2 contributions that will overlap with the peaks from NiO_x. This, together with the fact that the Ni $2p_{3/2}$ spectrum does not show clearly separated peaks makes it difficult to reliably identify all present NiO_x species in the UV-ozone treated, unannealed NiO_x film. Nevertheless, the large component towards higher binding energy suggests the presence of a significant amount of NiOOH.

The spectra of the NiO_x film annealed at 175°C followed by UV-ozone treatment are shown in Figure 4e and 4f. Since the wide scan did not show any signal from Si, we can confidently exclude any contributions from the substrate. Comparing the spectrum to that of the precursor, a clear asymmetry is visible in the O1s peak, which can be fitted to a new peak at higher binding energy, assigned to NiOOH.

When the NiO_x film has been annealed for one hour at 325°C, i.e. above the decomposition temperature of the nickel formate precursor,[47, 48] three main species are present in film, as can be seen clearly in the O 1s but also in the Ni $2p_{3/2}$ spectrum. Figure 4g and 4h show spectra of the films after UV-ozone treatment while Figure 4i and 4j show spectra only after thermal annealing. NiO, $Ni(OH)_2/Ni_2O_3$, and NiOOH are present in the film. Upon UV-ozone treatment, the NiO component is suppressed while the NiOOH component increases.

From this we conclude that only when we anneal the films at high temperature does NiO form in any significant amounts. UV-ozone treatment on the other hand promotes the formation of NiOOH. This is in agreement with previous studies of O_2-plasma and UV-ozone treated NiO_x.[34, 38, 42, 49]

The contact potential difference (CPD) values measured by Kelvin probe of NiO_x films on ITO are shown in Figure 5a. Prior to the UV-ozone treatment, the CPD varies between -350 and +50 mV with annealing temperature. After the NiO_x films have been UV-ozone treated, the CPD increases to +300 mV for all the films, independent of any preceding thermal annealing. Even further increase of contact potential difference (CPD) was observed for a freshly UV-ozone activated NiO_x film (Figure 5b). Directly after activation the CPD was about 960 mV higher and 30 min later the CPD is still 690 mV higher than before activation. The extrapolation by an exponential decay yields an equilibrium value of CPD which is more than half a volt above the CPD value of a non-activated film. No change in CPD was observed by spin coating pure oDCB, which excludes interaction between the activated surface and the used solvent during active layer spincoating.

Modification of the NiO_x work function has previously been demonstrated using O_2-plasma, increasing the work function by 0.5-0.8 eV.[27, 33, 34] The increase in work function that we observe here as a result of UV-ozone treatment is in the same range; assuming a work function for the gold reference probe of 4.8 eV, a freshly activated NiO_x film has a work

function of up to 5.6 eV. In comparison, reported values for the PEDOT:PSS work function, typically vary between 4.3 and 5.2 eV.[50-52]

The increased work function of NiO_x films upon O_2-plasma or UV-ozone treatment has been attributed in previous studies to a strong dipole due to the formation of NiOOH at the surface.[34, 38, 42, 53] The increase in work function of the UV-ozone treated NiO_x films that we observe here is therefore in agreement with our XPS results that indicate that NiOOH is formed as a result of the UV-ozone treatment.

From the XPS analysis it can be seen that high temperature annealing produces NiO, whereas the XPS, UV-Vis and CPD measurements together indicate that the UV-ozone treatment produces NiOOH. In other words, it is not NiO that is required to make a good HTL. In fact, as can be seen by comparing Figure 4g and 4h to Figure 4i and 4j, the UV-ozone treatment of NiO_x films annealed at 325°C reduces the amount of NiO while at the same time improving the solar cell performance. This improved performance correlates with the increased work function of the NiO_x films after the UV-ozone treatment (Figure 5); all solar cells with UV-ozone treated NiO_x outperform PEDOT:PSS and all UV-ozone treated NiO_x films have a higher work function, regardless of any previous annealing.

Energy level matching of the HOMO of the donor material and the work function of the HTL is important to provide efficient hole-collection at the anode as well as good charge injection. Solar cells utilizing polymers with deep HOMO energy levels have been shown to benefit from high work function HTLs.[33, 37, 38] Since TQ1 has a relatively deep HOMO (5.7 eV as measured by square wave voltammetry[43]), the high work function UV-ozone treated NiO_x is advantageous over PEDOT:PSS as the HTL for TQ1-based solar cells. Improvements of the device performance when replacing PEDOT:PSS with O_2-plasma or UV-ozone treated NiO_x has previously been correlated with the increased work function of the HTL.[27, 33, 37, 38, 42, 53]

Although the solar cells with UV-ozone treated NiO_x HTL all display a similar performance, the question remains as to whether they are stable and whether their stability depends on the annealing temperature. Lima et al. have shown for organic solar cells using solution processed V_2O_5 HTL that while VO_x films that contain residual precursor have similar performance compared to stoichiometric V_2O_5, the presence of residual precursor does have an adverse effect on the stability.[54] We cannot exclude that the NiO_x films synthesized at low temperature followed by UV-ozone treatment contain residual precursor, even though UV-ozone is known for its efficient decomposition and removal of organic molecules from surfaces. NiO_x film synthesized at high temperature, on the other hand, are less likely to contain undecomposed precursor.

In order to investigate the effect of the choice of HTL on the active layer morphology, TQ1:$PC_{70}BM$ blend films spincoated on NiO_x and on PEDOT:PSS respectively were imaged by AFM. No significant difference in surface topography was observed (Figure S3 of the supplementary material). From this we conclude that the lateral morphology is insensitive to our choice of HTL. Germack et al.[55] have previously shown that large differences in the surface energy of the substrate can affect the vertical morphology of poly-hexylthiophene (P3HT):PCBM blends. However, since the surface energy of NiO_x and PEDOT:PSS are similar,[56] we deem it unlikely that active layers spincoated on NiO_x and PEDOT:PSS would have significantly different vertical composition profiles.

4. Conclusions

Solar cells utilizing solution processed NiO_x HTLs have been made that outperform the solar cells with the standard PEDOT:PSS HTL prepared in this study. By subjecting a nickel formate precursor to UV-ozone treatment, high performing NiO_x HTLs can be created in a way that do not require any high temperature annealing. Upon UV-ozone exposure NiOOH is

formed at the surface, in contrast to high temperature annealing that promotes the formation of NiO. The UV-ozone treated NiO_x films all display high work function that do not depend on the preceding thermal annealing. The enhanced performance and higher FF of solar cells with UV-ozone treated NiO_x HTLs is attributed to improved energy level matching between the donor polymer HOMO and the HTL work function that provide efficient hole-collection and charge injection at the anode.

Acknowledgements

The authors thank the beamline staff at D1011, MAX-IV Laboratory, for valuable technical advice with the XPS experiments. E.M. acknowledges funding from the Swedish Energy Council, contract number 38327-1, and the Swedish Research Council, grant 2015-03778, and financial support from the Göran Gustafsson Foundation for Research in Natural Sciences and Medicine. The research was carried out within the framework of the COST Action MP1307 StableNextSol. L.E. greatly acknowledges financial support from the ÅForsk foundation.

References

1 S. H. Liao, H. J. Jhuo, P. N. Yeh, Y. S. Cheng, Y. L. Li, Y. H. Lee, S. Sharma and S. A. Chen, *Sci. Rep.*, **2014**, 4, 6813.

2 Z. He, B. Xiao, F. Liu, H. Wu, Y. Yang, S. Xiao, C. Wang, T. P. Russell and Y. Cao, *Nat. Photonics*, **2015**, 9, 174-179.

3 V. Vohra, K. Kawashima, T. Kakara, T. Koganezawa, I. Osaka, K. Takimiya and H. Murata, *Nat. Photonics*, **2015**, 9, 403-408.

4 J. D. Chen, C. Cui, Y. Q. Li, L. Zhou, Q. D. Ou, C. Li, Y. Li and J. X. Tang, *Adv. Mater.*, **2015**, 27, 1035-1041.

5 Y. Liu, J. Zhao, Z. Li, C. Mu, W. Ma, H. Hu, K. Jiang, H. Lin, H. Ade and H. Yan, *Nat. Commun.*, **2014**, 5, 1-8.

6 R. Søndergaard, M. Hösel, D. Angmo, T. T. Larsen-Olsen and F. C. Krebs, *Mater. Today*, **2012**, 15, 36-49.

7 I. J. Kramer and E. H. Sargent, *ACS Nano*, **2011**, 5, 8506-8514.

8 F. Wang, Z. a. Tan and Y. Li, *Energy Environ. Sci.*, **2015**, 8, 1059-1091.

9 W. C. Choy and D. Zhang, *Small*, **2016**, 12, 416-431.

10 M. P. de Jong, L. J. van Ijzendoorn and M. J. A. de Voigt, *Appl. Phys. Lett.*, **2000**, 77, 2255-2257.

11 K. Kawano, R. Pacios, D. Poplavskyy, J. Nelson, D. D. C. Bradley and J. R. Durrant, *Sol. Energy Mater. Sol. Cells*, **2006**, 90, 3520-3530.

12 M. Jørgensen, K. Norrman and F. C. Krebs, *Sol. Energy Mater. Sol. Cells*, **2008**, 92, 686-714.

13 K. Norrman, M. V. Madsen, S. A. Gevorgyan and F. C. Krebs, *J. Am. Chem. Soc.*, **2010**, 132, 16883-16892.

14 M. Jørgensen, K. Norrman, S. A. Gevorgyan, T. Tromholt, B. Andreasen and F. C. Krebs, *Adv. Mater.*, **2012**, 24, 580-612.

15 A. K. K. Kyaw, X. W. Sun, C. Y. Jiang, G. Q. Lo, D. W. Zhao and D. L. Kwong, *Appl. Phys. Lett.*, **2008**, 93, 221107.

16 D. W. Zhao, P. Liu, X. W. Sun, S. T. Tan, L. Ke and A. K. K. Kyaw, *Appl. Phys. Lett.*, **2009**, 95, 153304.

17 Y. Sun, C. J. Takacs, S. R. Cowan, J. H. Seo, X. Gong, A. Roy and A. J. Heeger, *Adv. Mater.*, **2011**, 23, 2226-2230.

18 J. Kim, H. Kim, G. Kim, H. Back and K. Lee, *ACS Appl. Mater. Interfaces*, **2014**, 6, 951-957.

19 B. Li, H. Ren, H. Yuan, A. Karim and X. Gong, *ACS Photonics*, **2014**, 1, 87-90.

20 V. Shrotriya, G. Li, Y. Yao, C.-W. Chu and Y. Yang, *Appl. Phys. Lett.*, **2006**, 88, 073508.

21 J.-S. Huang, C.-Y. Chou, M.-Y. Liu, K.-H. Tsai, W.-H. Lin and C.-F. Lin, *Org. Electron.*, **2009**, 10, 1060-1065.

22 Q. Xu, F. Wang, Z. Tan, L. Li, S. Li, X. Hou, G. Sun, X. Tu, J. Hou and Y. Li, *ACS Appl. Mater. Interfaces*, **2013**, 5, 10658-10664.

23 C. Tao, S. Ruan, G. Xie, X. Kong, L. Shen, F. Meng, C. Liu, X. Zhang, W. Dong and W. Chen, *Appl. Phys. Lett.*, **2009**, 94, 043311.

24 S. Han, W. S. Shin, M. Seo, D. Gupta, S.-J. Moon and S. Yoo, *Org. Electron.*, **2009**, 10, 791-797.

25 G. Ho Jung, K.-G. Lim, T.-W. Lee and J.-L. Lee, *Sol. Energy Mater. Sol. Cells*, **2011**, 95, 1146-1150.

26 M. D. Irwin, D. B. Buchholz, A. W. Hains, R. P. H. Chang and T. J. Marks, *Proc. Natl. Acad. Sci. USA*, **2008**, 105, 2783-2787.

27 J. J. Berry, N. E. Widjonarko, B. A. Bailey, A. K. Sigdel, D. S. Ginley and D. C. Olson, *IEEE J. Sel. Top. Quantum Electron.*, **2010**, 16, 1649-1655.

28 W. Yu, L. Shen, S. Ruan, F. Meng, J. Wang, E. Zhang and W. Chen, *Sol. Energy Mater. Sol. Cells*, **2012**, 98, 212-215.

29 C. C. Hsu, H. W. Su, C. H. Hou, J. J. Shyue and F. Y. Tsai, *Nanotechnology*, **2015**, 26, 385201.

30 J. W. Shim, C. Fuentes-Hernandez, A. Dindar, Y. Zhou, T. M. Khan and B. Kippelen, *Org. Electron.*, **2013**, 14, 2802-2808.

31 J. Kettle, H. Waters, M. Horie and S. W. Chang, *J. Phys. D: Appl. Phys.*, **2012**, 45, 125102.

32 R. Betancur, M. Maymó, X. Elias, L. T. Vuong and J. Martorell, *Sol. Energy Mater. Sol. Cells*, **2011**, 95, 735-739.

33 K. X. Steirer, P. F. Ndione, N. E. Widjonarko, M. T. Lloyd, J. Meyer, E. L. Ratcliff, A. Kahn, N. R. Armstrong, C. J. Curtis, D. S. Ginley, J. J. Berry and D. C. Olson, *Adv. Energy Mater.*, **2011**, 1, 813-820.

34 E. L. Ratcliff, J. Meyer, K. X. Steirer, A. Garcia, J. J. Berry, D. S. Ginley, D. C. Olson, A. Kahn and N. R. Armstrong, *Chem. Mater.*, **2011**, 23, 4988-5000.

35 A. Garcia, G. C. Welch, E. L. Ratcliff, D. S. Ginley, G. C. Bazan and D. C. Olson, *Adv. Mater.*, **2012**, 24, 5368-5373.

36 J. R. Manders, S.-W. Tsang, M. J. Hartel, T.-H. Lai, S. Chen, C. M. Amb, J. R. Reynolds and F. So, *Adv. Funct. Mater.*, **2013**, 23, 2993-3001.

37 K. X. Steirer, J. P. Chesin, N. E. Widjonarko, J. J. Berry, A. Miedaner, D. S. Ginley and D. C. Olson, *Org. Electron.*, **2010**, 11, 1414-1418.

38 Z. Zhai, X. Huang, M. Xu, J. Yuan, J. Peng and W. Ma, *Adv. Energy Mater.*, **2013**, 3, 1614-1622.

39 F. Jiang, W. C. Choy, X. Li, D. Zhang and J. Cheng, *Adv Mater*, **2015**, 27, 2930-2937.

40 K. Sugiyama, H. Ishii, Y. Ouchi and K. Seki, *J. Appl. Phys.*, **2000**, 87, 295-298.

41 S. Y. Kim, *J. Appl. Phys.*, **2004**, 95, 2560-2563.

42 F. Wang, G. Sun, C. Li, J. Liu, S. Hu, H. Zheng, Z. Tan and Y. Li, *ACS Appl. Mater. Interfaces*, **2014**, 6, 9458-9465.

43 E. Wang, L. Hou, Z. Wang, S. Hellstrom, F. Zhang, O. Inganäs and M. R. Andersson, *Adv. Mater.*, **2010**, 22, 5240-5244.

44 R. Hansson, C. Lindqvist, L. K. Ericsson, A. Opitz, E. Wang and E. Moons, *Phys Chem Chem Phys*, **2016**, 18, 11132-8.

45 K. S. Kim and N. Winograd, *Surf. Sci.*, **1974**, 43, 625-643.

46 H. W. Nesbitt, D. Legrand and G. M. Bancroft, *Phys. Chem. Miner.*, **2000**, 27, 357-366.

47 B. Xia, I. W. Lenggoro and K. Okuyama, *J. Am. Ceram. Soc.*, **2001**, 84, 1425-1432.

48 K. X. Steirer, R. E. Richards, A. K. Sigdel, A. Garcia, P. F. Ndione, S. Hammond, D. Baker, E. L. Ratcliff, C. Curtis, T. Furtak, D. S. Ginley, D. C. Olson, N. R. Armstrong and J. J. Berry, *J. Mater. Chem. A*, **2015**, 3, 10949-10958.

49 J. Zhang, J. Wang, Y. Fu, B. Zhang and Z. Xie, *J. Mater. Chem. C*, **2014**, 2, 8295-8302.

50 N. Koch, A. Elschner, J. P. Rabe and R. L. Johnson, *Adv. Mater.*, **2005**, 17, 330-335.

51 G. Greczynski, T. Kugler and W. R. Salaneck, *J. Appl. Phys.*, **2000**, 88, 7187-7191.

52 N. Koch, A. Kahn, J. Ghijsen, J. J. Pireaux, J. Schwartz, R. L. Johnson and A. Elschner, *Appl. Phys. Lett.*, **2003**, 82, 70-72.

53 E. L. Ratcliff, J. Meyer, K. X. Steirer, N. R. Armstrong, D. Olson and A. Kahn, *Org. Electron.*, **2012**, 13, 744-749.

54 F. A. S. Lima, M. J. Beliatis, B. Roth, T. R. Andersen, A. Bortoti, Y. Reyna, E. Castro, I. F. Vasconcelos, S. A. Gevorgyan, F. C. Krebs and M. Lira-Cantu, *APL Mater.*, **2016**, 4, 026104.

55 D. S. Germack, C. K. Chan, B. H. Hamadani, L. J. Richter, D. A. Fischer, D. J. Gundlach and D. M. DeLongchamp, *Appl. Phys. Lett.*, **2009**, 94, 233303.

56 N. E. Widjonarko, P. Schulz, P. A. Parilla, C. L. Perkins, P. F. Ndione, A. K. Sigdel, D. C. Olson, D. S. Ginley, A. Kahn, M. F. Toney and J. J. Berry, *Adv. Energy Mater.*, **2014**, 4, 1301879.

Table 1. Device parameters of photovoltaic devices of ITO/HTL/TQ1:$PC_{70}BM$/LiF/Al. Mean values ± standard deviations, each from 8-10 devices are shown. Each substrate has two devices and each type of sample was prepared in at least 4 different preparation runs. NiO_x annealing times are 24 h unless otherwise stated.

Sample	J_{SC} (mA/cm^2)	V_{OC} (V)	FF (%)	PCE (%)
NiO_x RT	~10^{-2}	~10^{-4}	24.3 ± 0.7	~10^{-6}
NiO_x 100°C	~10^{-2}	0.1 ± 0.04	25.4 ±1.1	~10^{-4}
NiO_x 175°C	0.1 ± 0.03	0.29 ± 0.09	18.4 ± 2.7	~10^{-3}
NiO_x 325°C 0.5 h	9.08 ± 0.48	0.56 ± 0.05	62.1 ± 2.0	3.16 ± 0.21
NiO_x 325°C 2 h	9.80 ± 0.22	0.71 ± 0.016	62.8 ± 0.8	4.34 ± 0.21
NiO_x RT+UV	9.95 ± 0.44	0.85 ± 0.015	65.5 ± 2.1	5.54 ± 0.41
NiO_x 100°C + UV	9.98 ± 0.38	0.86 ±0.010	62.7 ± 5.1	5.40 ± 0.45
NiO_x 175°C + UV	10.21 ± 0.26	0.88 ±0.004	67.9 ± 2.6	6.08 ±0.36
NiO_x 325°C 0.5 h + UV	9.48 ± 0.59	0.86 ±0.039	66.2 ± 1.6	5.39 ±0.57
PEDOT:PSS	10.55 ± 0.37	0.87 ± 0.014	58.2 ± 0.3	5.31 ± 0.27

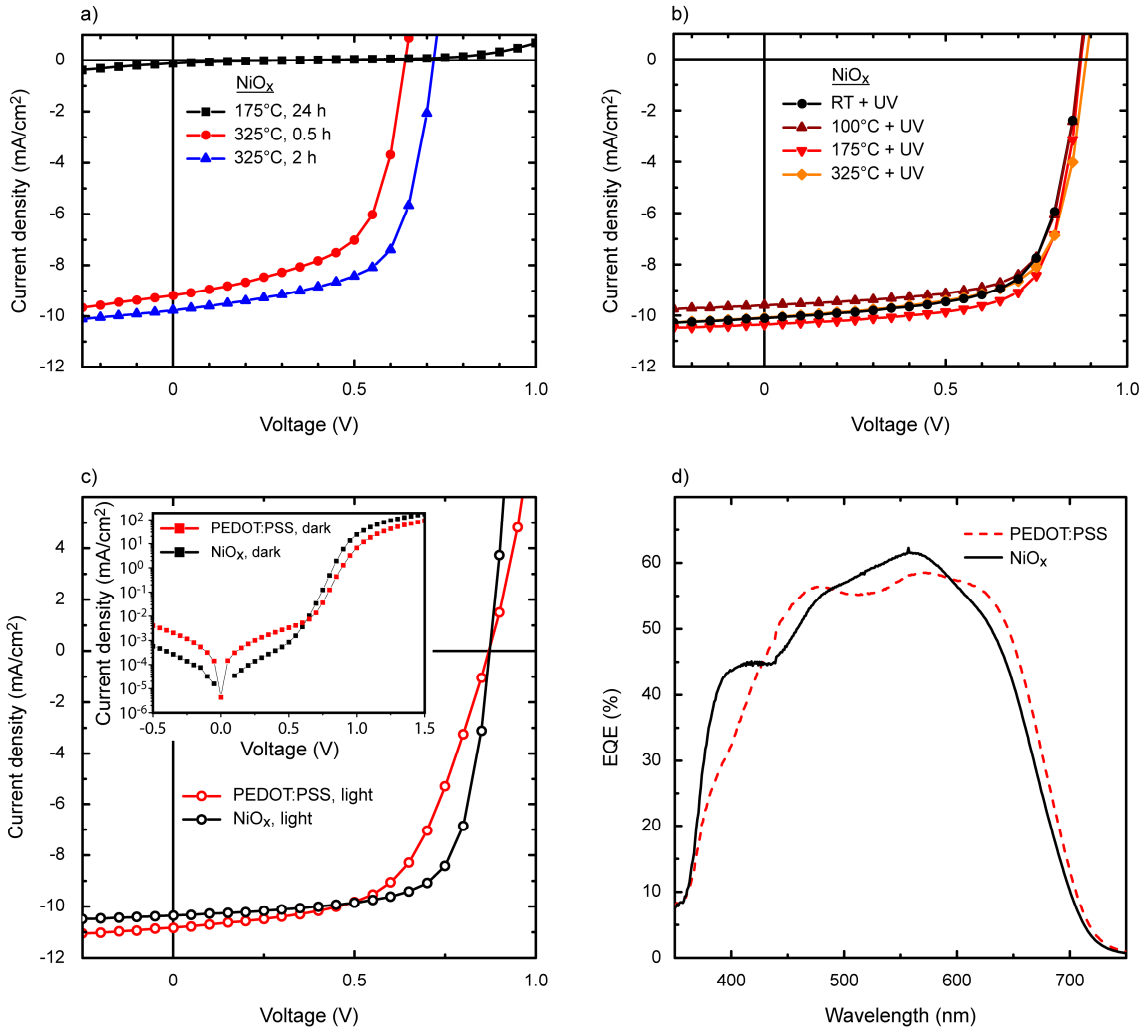

Figure 1. Current-voltage characteristics under illumination (a-c) and EQE (d) of TQ1:$PC_{70}BM$ solar cells utilizing different HTLs. The effect of the annealing temperature for NiO_x films without subsequent UV-ozone treatment is shown in a) while the effect of annealing temperature prior to UV-ozone treatment is shown in b). A solar cell using the best performing NiO_x HTL (175°C+UV) is compared to one using PEDOT:PSS in c), while d) compares the EQE of solar cells using the best performing NiO_x to PEDOT:PSS.

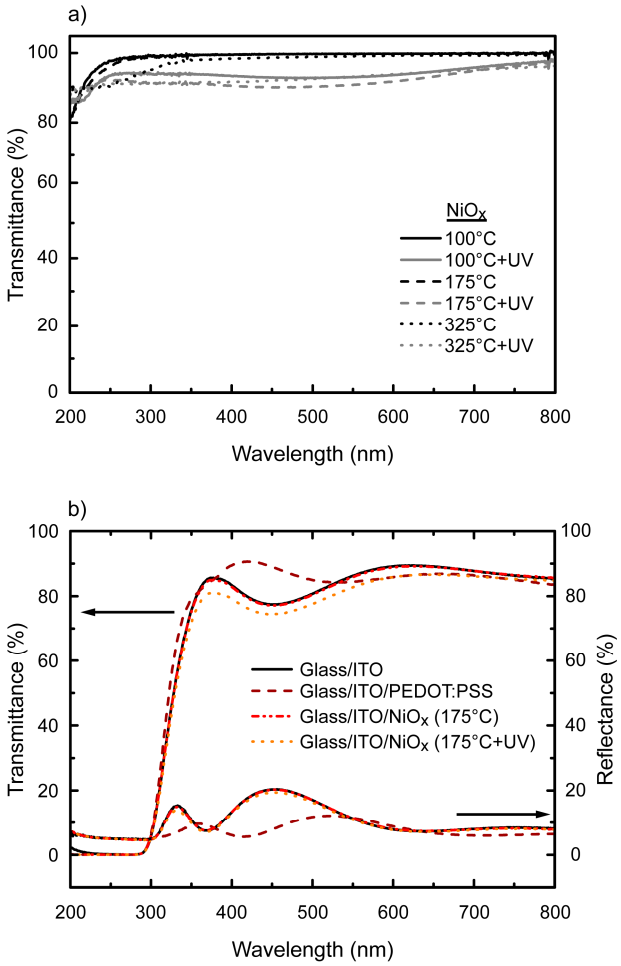

Figure 2. Optical properties of the NiO_x layers. a) Transmittance of different NiO_x thin films on quartz. b) Transmittance and reflectance comparing bare glass/ITO to that covered by PEDOT:PSS, NiO_x annealed at 175°C with and without subsequent UV-ozone exposure.

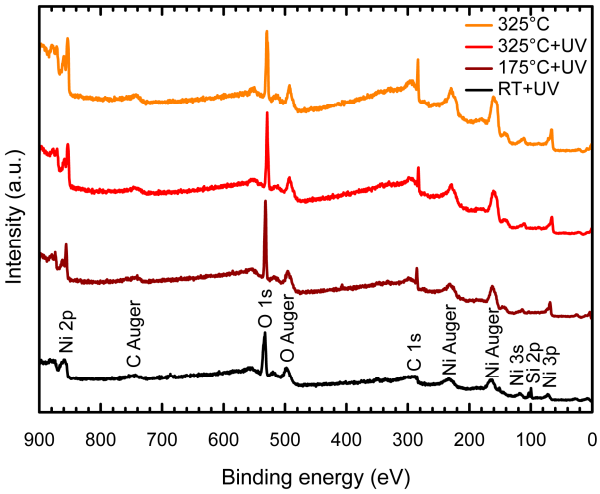

Figure 3. XPS survey scan of NiO_x thin films, annealed at different temperatures followed by UV-ozone treatment, and annealed at 325°C without UV-ozone treatment.

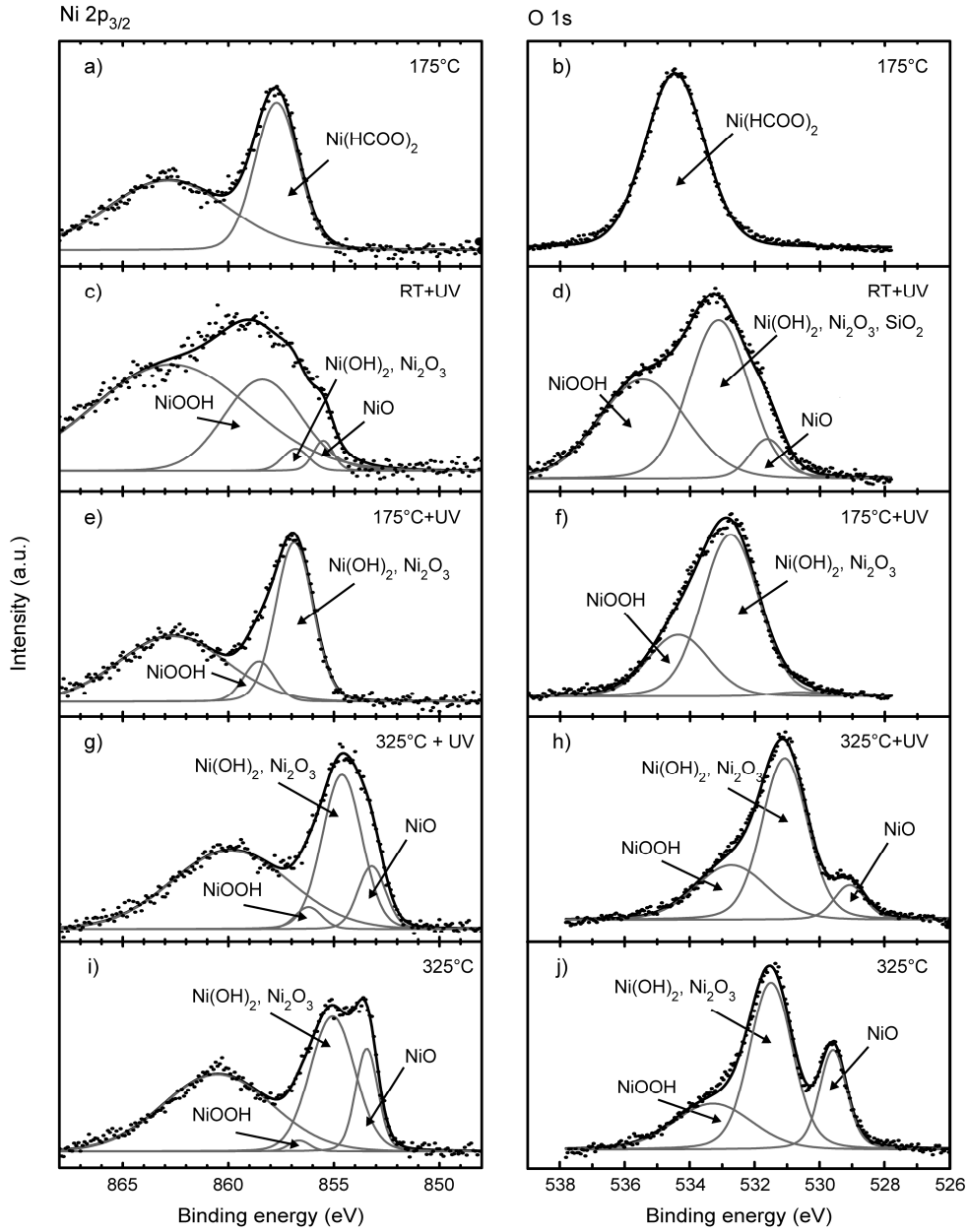

Figure 4. Ni $2p_{3/2}$ and O 1s core level spectra of NiO_x thin films prepared under different conditions.

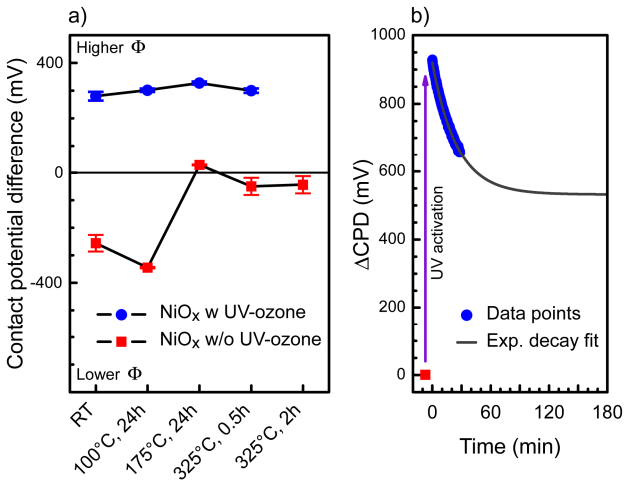

Figure 5. a) CPD of NiO_x thin films as a function of annealing temperature with (blue circles) and without (red squares) 3 h of UV-ozone treatment. b) Change in CPD of a NiO_x thin film as a result of UV-ozone activation.

- NiO_x hole transport layers prepared without need for high temperature annealing.
- UV-ozone treatment increases NiO_x work function and forms NiOOH.
- High work function leads to improved energy level matching.
- Polymer solar cells with NiO_x HTL demonstrate enhanced fill factor.